ELSEVIER

Journal of Alloys and Compounds 320 (2001) 228–233

Journal of ALLOYS AND COMPOUNDS

www.elsevier.com/locate/jallcom

Thermodynamic optimisation of the Pb–Tl binary system

S.G. Fries[a,*], I. Ansara[b], H.L. Lukas[c]

[a]*ACCESS e.V., RWTH-Aachen, Intzestr 5, D-52072 Aachen, Germany*

[b]*Laboratoire de Thermodynamique et de Physico-Chimie Métallurgiques ENSEEG, B.P. 75, F-38402 Saint-Martin-d'Hères Cedex, France*

[c]*Max-Planck-Institut für Metallforschung and Institut für Nichtmetallische Anorganische Materialien, University Stuttgart, Heisenbergstr. 5, D-70569 Stuttgart, Germany*

Abstract

The phase diagram of the Pb–Tl binary system is experimentally well determined. Experimental thermodynamic values for all the phases involved are also available. For the liquid phase the temperature dependence of the enthalpy of mixing is also determined. In the present contribution, a consistent set of Gibbs energy functions of all the phases is obtained using the Redlich–Kister polynomial. The adjustable model parameters were determined by least-squares fit to the experimental data. A satisfactory agreement between experimental and calculated values is observed.

Keywords: CALPHAD; Thermodynamic modelling; Rapid solidification; Gulliver–Scheil model; Pb–Tl alloys

1. Experimental data

The Pb–Tl phase diagram exhibits three solid solution phases, namely, *fcc*, *bcc* and *hcp*, starting from the corresponding phases of the pure elements. *Bcc* and *hcp* solid solution phases are restricted to Tl-rich compositions ($x_{Tl} > 0.93$), whereas the *fcc* solution phase exhibits a very large homogeneity range from pure Pb to $x_{Tl} = 0.9$. The liquidus presents a maximum, where the *fcc* phase melts congruently at 653 K and $x_{Tl} = 0.625$. The *bcc* solid solution forms peritectically at 585 K from Tl-rich liquid and *fcc* phases and decomposes eutectoidally at about 453 K into Tl-rich *fcc* and *hcp* phases.

Liquidus temperatures were first measured by Heycock and Neville [1] in the Tl-rich composition range using thermal analysis. They observed a raise of the freezing temperatures on small additions of Pb to Tl. Later Kurnakov and Puschin [2], Lewkonja [3], Di Capua [4], Kurnakov and Korenev [7], Predel and Schürmann [18] determined the liquidus and peritectic temperatures. Predel and Schürmann [18] also measured solidus temperatures over the entire composition range. The congruent melting temperature differs by 7 K and the peritectic temperature by 2.5 K between these studies. The two-phase field between the *bcc* and *hcp* Tl-rich phases was determined by electrical resistivity measurements [5]. For the eutectoid decomposition of the *bcc* phase a value of 542 K was interpolated between DTA effects on cooling and heating [20]. The enthalpy of formation of liquid alloys was measured by Wittig and Scheidt [12] at 673 K, by Scheil and Lukas [13] at three temperatures from 635 to 779 K, and by Badawi et al. [24] at 755 K, over the entire composition range. The enthalpy of melting was measured by Nagasaki and Maesono [16], Predel and Mohs [17], Predel and Schürmann [18] in the same composition range.

The chemical potential of Tl in liquid alloys was measured by emf by Hildebrand and Sharma [6] at 711, 773 and 836 K and by Kundys et al. [14] at 673, 773 and 873 K. The same state function was determined by vapour pressure by Stachura et al. [15] at 848 K and by Lyubman [19] at 1273 and 1373 K. The chemical potential of Pb in liquid alloys was also determined by vapour pressure by Nakazawa and Yazawa [21] at 858 K and by Lyubman et al. [19] at 1273 and 1373 K. Hildebrand and Sharma [6], Kundys et al. [14], Stachura et al. [15] and Nakazawa and Yazawa [21] investigated alloys over the entire composition range, whereas Lyubman et al. [19] measured from $x_{Tl} = 0$ to 0.5.

Oelander [8] measured the chemical potential of Tl in the *fcc* solid solution at 523 K between 15 and 92 mol-% Tl.

The heat content ($H(T)$–$H(298\ K)$) of two alloys ($x_{Tl} = 0.63$ and 0.8754) was measured by drop calorimetry [9].

Abbasov et al. [22] measured heat capacities of solid alloys and postulated several ordering phases. They found minima in C_p versus T curves corresponding to exothermic

*Corresponding author.

0925-8388/01/$ – see front matter
PII: S0925-8388(00)01492-4

Table 1
Experimental data[a]

Ref.	Experimental method	Value	Temperature (K)	Mole % Tl	Used
[1]	therm. anal.	liquidus	577–582	97–100	+
[2]	thermal	liquidus	582–653	0–100	+
	analysis	peritectic	583		−
[3]	thermal	liquidus	578–650	0–100	+
	analysis	peritectic	582.5		−
[4]	thermal	liquidus	579–652	67–100	+
	analysis	peritectic	584		−
[5]	electric	$\alpha+\beta$–Tl	439–500	95–100	+
	resistivity	two-phase equil.			
[7]	therm. anal.	liquidus	607–657	10–75	+
[18]	thermal	liq.+solidus	577–654	0–100	+
	analysis	peritectic	585		+
[20]	DTA	eutectoid	442		+
[9]	calorimetry	$H(T)-H(298\ \mathrm{K})$	466–883	63, 85.54	+
[12]	calorimetry	ΔH^{liq}	673	5–90	+
[13]	calorimetry	ΔH^{liq}	635–779	5–90	+
[24]	calorimetry	H^{liq}	775	0–100	−
[16]	calorimetry	$H^{liq}-H^{sol}$	576–651	0–100	+
[17]	calorimetry	$H^{liq}-H^{sol}$	604–635	4–50	+
[18]	calorimetry	$H^{liq}-H^{sol}$	576–650	0–100	+
[6]	emf	μ_{Tl}^{liq}	711, 773, 836	4–88	+
[8]	emf	μ_{Tl}^{fcc}	523	15–92	+
[14]	emf	μ_{Tl}^{liq}	673, 773, 873	5–90	+
[15]	vap. press.	μ_{Tl}^{liq}	848	18–79	+
[19]	vap. press.	μ_{Pb}^{liq}, μ_{Tl}^{liq}	1273, 1373	3–50	−
[21]	vap. press.	μ_{Pb}^{liq}	858	10–90	+
[22]	calorimetry	C_p	323–823	0–100	−

[a] The last column indicates whether the values were used '+' or not used '−' in the optimisation.

effects during heating. Following equilibrium states during heating only endothermic processes are possible, thus these effects can only be due to annealing out of quenched non-equilibrium states. These values, therefore, cannot be used for the optimisation.

All the experimental data are summarised in Table 1. The crystal structures and phase characteristics are presented in Table 2.

2. Thermodynamic description

2.1. Models

The pure solid elements at 298.15 K in their stable form were chosen as the reference state of the system. For the thermodynamic functions of the pure elements in their stable and metastable states, the SGTE phase stability equations published by Dinsdale [23] were used.

Table 2
Crystal structures and phase descriptions

System	Phase	Prototype	Pearson symbol	Space group	Struktur Bericht
Pb–Tl	(Pb)-*fcc*	Cu	*cF4*	$Fm\bar{3}m$	*Al*
	(Tl)-*bcc*	W	*c12*	$Im\bar{3}m$	*A2*
	(Tl)-*hcp*	Mg	*hP2*	$P6_3/mmc$	*A3*

The excess terms of all the phases were modelled by the Redlich–Kister formula [10]. The equations are given in the form (the superscript ϕ stands for the phase name):

$$G^{\phi}(T) - H^{\mathrm{SER}}(298\ \mathrm{K}) = {}^{\mathrm{ref}}G^{\phi} + {}^{\mathrm{id}}G + {}^{\mathrm{xs}}G^{\phi} \qquad (0.1)$$

where:

$${}^{\mathrm{ref}}G^{\phi} = [{}^{0}G^{\phi}_{\mathrm{Pb}}(T) - H^{\mathrm{SER}}_{\mathrm{Pb}}(298.15\ \mathrm{K})]\cdot x_{\mathrm{Pb}} + [{}^{0}G^{\phi}_{\mathrm{Tl}}(T) - H^{\mathrm{SER}}_{\mathrm{Tl}}(298.15\ \mathrm{K})]\cdot x_{\mathrm{Tl}}$$

$${}^{\mathrm{id}}G^{\phi} = R\cdot T\cdot[x_{\mathrm{Pb}}\cdot\ln(x_{\mathrm{Pb}}) + x_{\mathrm{Tl}}\cdot\ln(x_{\mathrm{Tl}})]$$

$${}^{\mathrm{xs}}G^{\phi} = x_{\mathrm{Pb}}\cdot x_{\mathrm{Tl}}\cdot[{}^{0}L^{\phi}_{\mathrm{Pb,Tl}} + {}^{1}L^{\phi}_{\mathrm{Pb,Tl}}\cdot(x_{\mathrm{Pb}}-x_{\mathrm{Tl}}) + {}^{2}L^{\phi}_{\mathrm{Pb,Tl}}\cdot(x_{\mathrm{Pb}}-x_{\mathrm{Tl}})^2\ldots]$$

with

$${}^{0}L^{\phi}_{\mathrm{Pb,Tl}} = a_0 + b_0\cdot T + c_0\cdot T\cdot\ln T$$

$${}^{1}L^{\phi}_{\mathrm{Pb,Tl}} = a_1 + b_1\cdot T$$

$${}^{2}L^{\phi}_{\mathrm{Pb,Tl}} = a_2 + b_2\cdot T$$

2.2. Optimisation

The different experimental data for the temperature of the peritectic invariant equilibrium deviate slightly; the value reported by Predel and Schürmann [18] was selected. The values of the chemical potentials reported by Lyubman and Senyuta [19], measured at high temperatures, combined with those measured at lower temperatures [6,14,15,21], lead to a much higher temperature dependence of the Gibbs energy description than the one derived from the enthalpy of mixing data. The data of Ref. [19], therefore, were not used for the optimisation.

The enthalpies of mixing reported by Wittig and Scheidt [12] and Scheil and Lukas [13] were directly measured by mixing the pure elements, which were already inside the calorimeter at the reaction temperature, whereas those of Badawi et al. [24] were determined by dropping the pure elements from room temperature into the calorimeter. The enthalpies of mixing were calculated from the measured heat effects by subtracting the heat contents of the pure elements. There is a discrepancy between the heat contents of the pure elements, $H^0_{Pb}(775\ K)-H^0_{Pb}(298\ K)$ and $H^0_{Tl}(775\ K)-H^0_{Tl}(298\ K)$, used by Badawi et al. [24] and those calculated from the SGTE unary data [23] by 860 and 400 J/mol respectively. The enthalpy of melting of pure Pb reported by Badawi et al. [24], 5473 J/mol, also disagrees with the SGTE value [23], 4774 J/mol, by 699 J/mol. Although the data of Badawi et al. [24] deviate only slightly from those of Wittig and Scheidt [12] and Scheil and Lukas [13], their use in the optimisation would virtually interpret the deviation as a temperature dependence of the mixing enthalpy and thus conflict with the temperature dependence measured by Scheil and Lukas [13]. Therefore, they were not used.

All the other experimental values where taken into account in the optimisation.

The *bcc* and *hcp* solid solutions have very limited homogeneity ranges and they extend over a narrow range of temperature. For the *hcp* phase, a single constant Redlich–Kister parameter was optimised, whereas for the *bcc* phase, as two different temperatures of the invariant equilibria are known, a Redlich–Kister parameter of the type ${}^0L^{bcc} = a + b \cdot T$ was chosen.

The liquid and *fcc* phases extend over very large composition ranges, so several Redlich–Kister parameters can be independently adjusted. As the temperature dependence of the enthalpy of mixing is known, at least one $T \cdot \ln(T)$ term can be adjusted for the liquid phase. Enthalpy and chemical potential values exist for liquid as well as for the solid phase. The enthalpy of the *fcc* phase is related to that of the liquid phase by the measured enthalpy of fusion. Thus, most of the Redlich–Kister parameters can be adjusted as linear functions of *T*. The optimal number of parameters must be determined by testing. Finally three parameters were found to be sufficient to describe the excess Gibbs energies of the liquid as well as of the *fcc* phases. The ${}^0L^{liq}$ parameter was selected as $a + b \cdot T + c \cdot T \cdot \ln T$, whereas the other five ones were set as $a + b \cdot T$.

The least squares optimisation was carried out by the program BINGSS [25].

Table 3
Results[a]

Phase	Parameter	a_v	b_v	c_v
liquid	${}^0L^{liq}_{Pb,Tl}$	−6453.40	27.23311	−3.394542
	${}^1L^{liq}_{Pb,Tl}$	313.01	0.59285	–
	${}^2L^{liq}_{Pb,Tl}$	538.29	0.87994	–
fcc	${}^0L^{fcc}_{Pb,Tl}$	−8182.59	3.92502	–
	${}^1L^{fcc}_{Pb,Tl}$	800.86	3.79107	–
	${}^2L^{fcc}_{Pb,Tl}$	1695.79	−2.22944	–
bcc	${}^0L^{bcc}_{Pb,Tl}$	−8746.72	5.31624	–
hcp	${}^0L^{hcp}_{Pb,Tl}$	−4345.49	–	–

[a] Excess parameters for the Pb–Tl system, given in J/mol. All phases are modelled with the Redlich–Kister formula.

3. Results and discussions

Table 3 presents the optimised coefficients for the liquid, *fcc*, *bcc*, and *hcp* phases.

Figs. 1 and 2 show the complete phase diagram and the enlarged Tl-rich side respectively, calculated from the present description. The agreement with the experimental data is very good.

Table 4 summarises calculated temperatures and phase compositions of the invariant equilibria.

Fig. 3 shows the calculated enthalpy of formation of liquid alloys at three temperatures compared with the experimental data. The data of Badawi et al. [24] do not deviate much from the other ones, but their use would interfere with the temperature dependence of $\Delta_{mix}H^{liq}$ given by the other values.

Fig. 4 presents the calculated enthalpies of fusion compared with the quite scattered experimental data. The

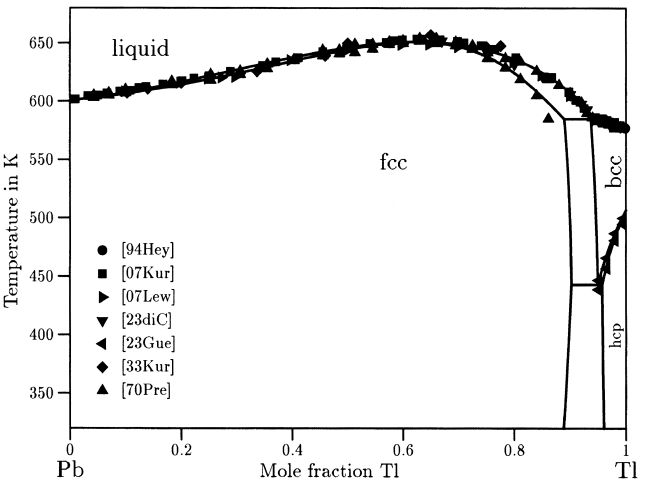

Fig. 1. Calculated and experimental phase diagram.

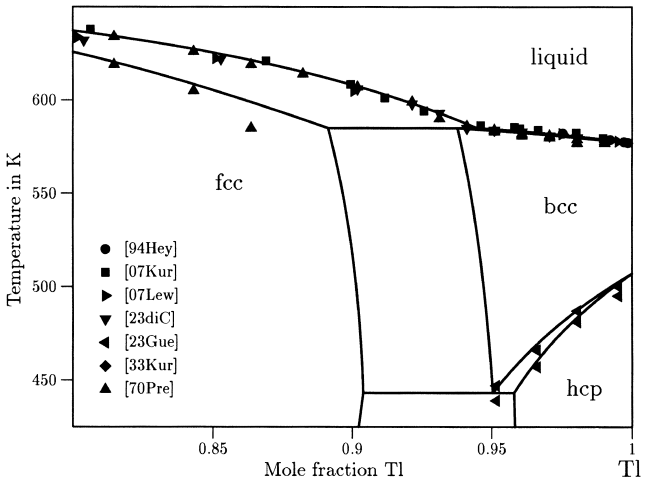

Fig. 2. Calculated and experimental phase diagram in the Tl-rich corner.

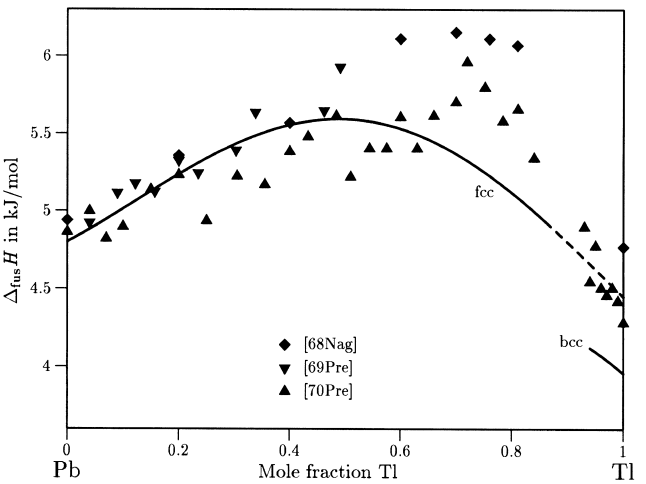

Fig. 4. Enthalpies of fusion of Pb–Tl alloys, extrapolated to 630 K.

Table 4
Invariant reactions

Reaction	Type	Compositions x_{Tl}			T/K
liquid⇌*fcc*	Congruent	0.625	0.625	–	651.1
liquid+*fcc*⇌*bcc*	Peritectic	0.944	0.889	0.937	585.0
bcc⇌*hcp*+*fcc*	Eutectoid	0.949	0.957	0.902	443.2

disagreement between the calculated curve and experimental values for $\Delta_{fus}H^{liquid\text{-}bcc}$ is mainly due to a disagreement between the enthalpy of melting values of pure Tl given by Nagasaki and Maesono [16] and Predel and Schürmann [18] with those selected in the SGTE pure element data set [23]. The calculated enthalpies of fusion of *fcc* alloys in the Tl-rich side also deviate from the experimental ones, mainly due to the SGTE phase stabilities of pure Tl. In Fig. 4 the calculated curve is extrapolated by a dashed line into the range where the *fcc* phase is not stable (86 to 100 at.% Tl). There it ends at the value of ${}^0H_{Tl}^{liquid}(T) - {}^0H_{Tl}^{fcc}(T)$ derived from the SGTE [23] enthalpy versus T description for the liquid and *fcc* phases. This situation, however, does not seem to be sufficient to require changes to the accepted SGTE [23] phase stabilities of pure Tl as the experimental values are quite scattered.

Fig. 5 shows the calculated heat content for two compositions as a function of temperature compared with experimental data. As no excess heat capacity was modelled for the *fcc* phase and as the difference between $C_{p,Pb}^{fcc}$ and $C_{p,Tl}^{fcc}$ is small, the calculated branches corresponding to the *fcc* phase virtually coincide for both alloys.

Figs. 6 and 7 show the calculated chemical potentials for both elements in the liquid phase at low and high temperatures respectively. In Fig. 6 the chemical potential of each element is calculated for one temperature only. The experimental points are shifted by the calculated difference $\mu_i^{liq}(T) - \mu_i^{liq}(T_0)$, where T is the temperature of measurement and T_0 that of the calculated curve. By this method the differences between experimental points and calculated curve are exactly the same as they would be between

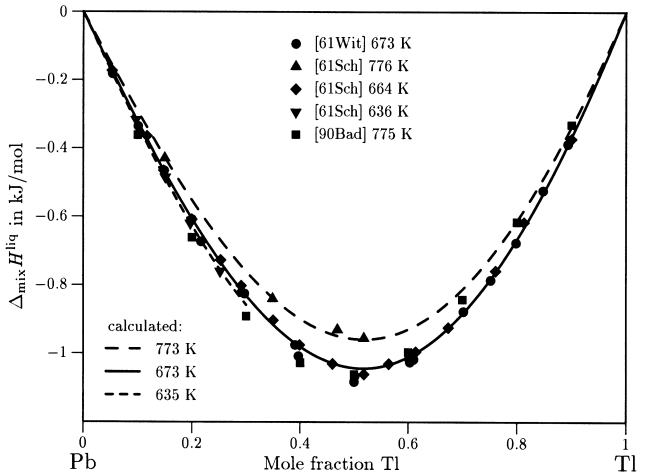

Fig. 3. Enthalpies of formation of liquid alloys, calculated at 635, 673 and 773 K.

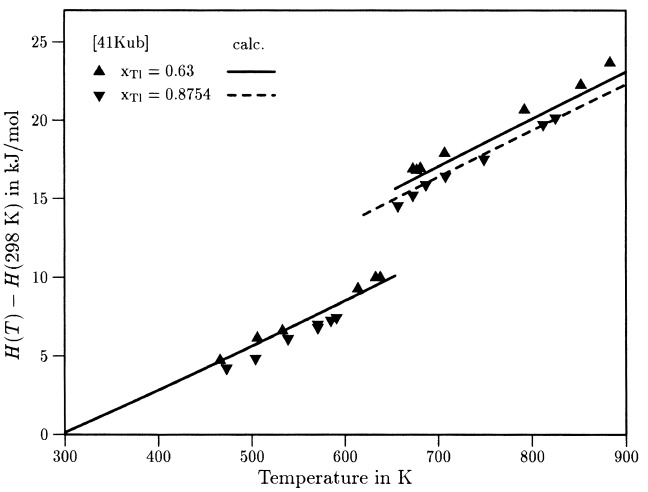

Fig. 5. Calculated and measured heat contents of two selected alloys.

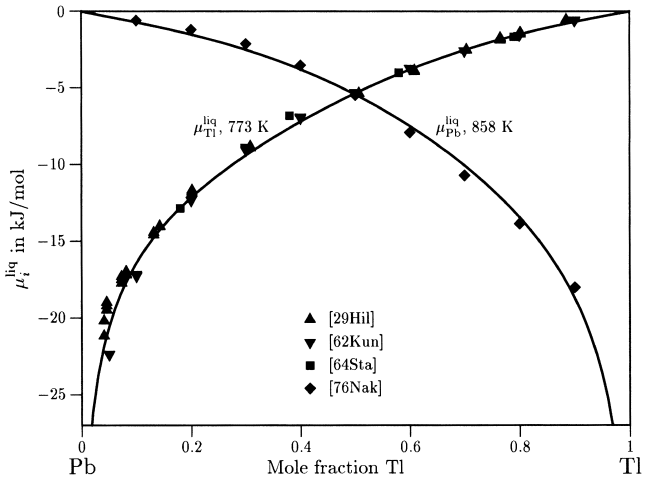

Fig. 6. Chemical potentials of Pb at 858 K and Tl at 773 K in the liquid phase.

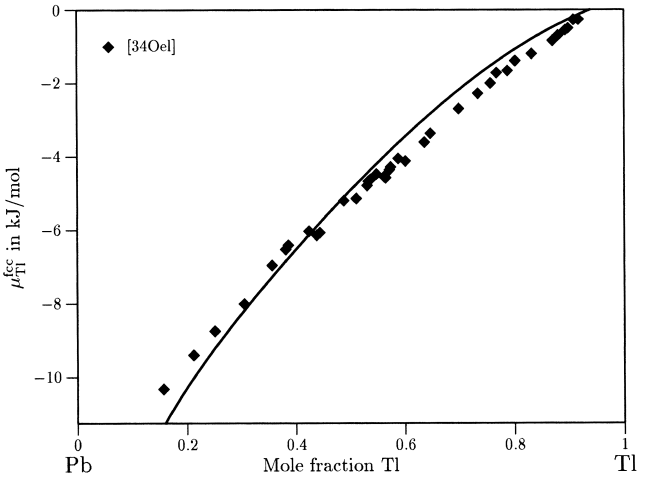

Fig. 8. Chemical potential of Tl in the *fcc* phase at 523 K.

unshifted points and curves calculated for the corresponding temperatures of measurement. By this method the figure is much clearer than with different curves for each temperature. The agreement with the experimental data in Fig. 6 is satisfactory. The values of [19] deviate quite significantly. The temperature dependence in the optimised description is based on the enthalpy measurements according to the relation: $d(\mu_i/T)/d(1/T)=H_i$. This relation usually gives more reliable temperature dependences than comparison of μ values measured at different temperatures.

Fig. 8 presents the calculated chemical potential of Tl in the *fcc* solid solution as a function of composition at 523 K. The curve agrees reasonably well with the experimental data.

It is interesting to comment on the reports concerning a superlattice ordering in the *fcc* phase. From X-ray diffraction studies, Tang and Pauling [11] assumed a ''strong indication'' of two ordered phases $PbTl_3$ and $PbTl_7$. These results were not confirmed by Predel [18], but they deduced an ordering tendency from their enthalpy measurements, near the composition $PbTl_3$, which ''however does not lead to a superlattice ordering''. The work of Abbasov et al. [22], which reports the existence of three intermetallic compounds, $PbTl_7$, $PbTl_3$ and Pb_3Tl_5 after a calorimetric study, is not performed in equilibrium conditions (see Experimental Data section) and, thus, does not enable to establish the existence of these phases.

An important application of thermodynamic assessments is their use in solidification simulations. In a study of the dynamic process of formation of cellular arrays in directional solidification, Li et al. [27] used a model alloy Pb-30%w Tl to verify the influence of different thermal gradients on the final microstructure pattern.

In their work, effective solute partition coefficients were extracted from macro-segregation experimental data. These data show a significant dependence on the solidification rates obtained by applying two different temperature gradients.

There a comparison with the Scheil approximation is interesting, which assumes no diffusion in the solid and infinitely rapid diffusion in the liquid.

Fig. 9 shows the calculated composition of the solid phase as a function of the already solidified fraction of the sample for the Pb-30%w Tl model alloy. It was calculated using the Scheil module of the Thermo-Calc software [26,28] and the thermodynamic description given in Table 3. For the rapid solidification, with a gradient of 40 K/cm, this calculation reproduces quite well the experimental data, whereas the slow crystallisation at 30 K/cm significantly deviates from the Scheil approximation. The solidified fraction was also calculated as a function of temperature, as shown in Fig. 10.

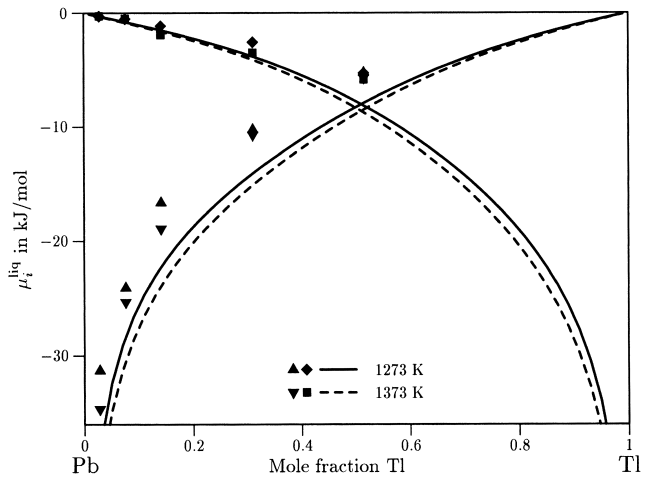

Fig. 7. Chemical potentials of Pb and Tl in the liquid phase at 1273 and 1373 K (experimental points [19]).

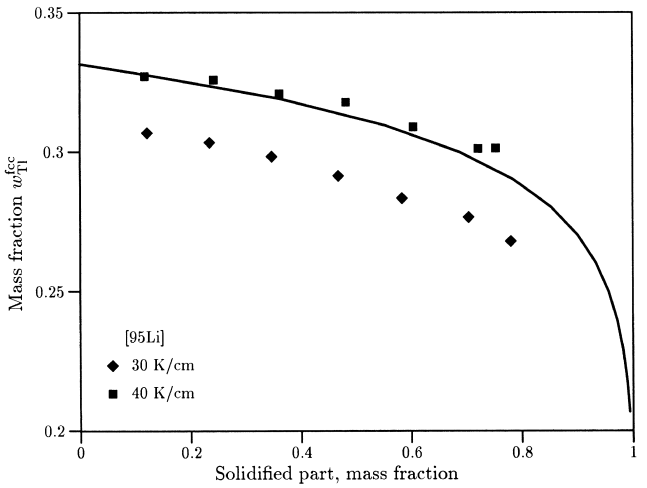

Fig. 9. Scheil calculation for a Pb-30%w Tl alloy, composition of solid versus solid fraction.

4. Conclusions

A complete set of analytical Gibbs energy functions is presented for all phases in the Pb–Tl binary system. The calculated quantities agree fairly well with the available experimental data. An application of these Gibbs energy functions is demonstrated by a Scheil solidification simulation.

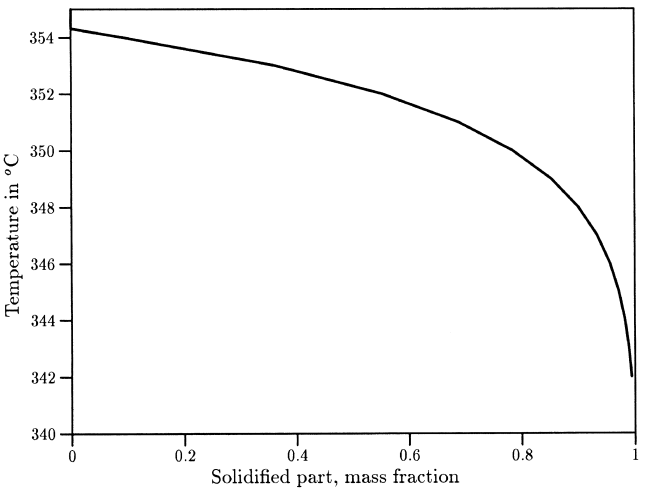

Fig. 10. Scheil calculation for a Pb-30%w Tl alloy, temperature versus solid fraction.

References

[1] C.T. Heycock, F.A. Neville, J. Chem. Soc. 65 (1894) 31–35.
[2] N.S. Kurnakov, N.A. Puschin, Z. Anorg. Chem. 52 (1907) 430–451.
[3] K. Lewkonja, Z. Anorg. Chem. 52 (1907) 452–456.
[4] C. Di Capua, Rendiconti Accademia Nationale Dei Liccei 23 (1923) 343–346.
[5] W. Guertler, A. Schuize, Z. Phys. Chem. 164 (1923) 269–300.
[6] J.H. Hildebrand, J.N. Sharma, J. Am. Chem. Soc. 51 (1929) 462–471.
[7] N.S. Kurnakov, N.I. Korenev, Izvest. Inst. Fiz.-Khim. Anal. 6 (1933) 47–68.
[8] A. Oelander, Z. Phys. Chem. 168 (1934) 274–282.
[9] O. Kubaschewski, Z. Elektrochem. 47 (1941) 475–484.
[10] O. Redlich, A.T. Kister, Indust. Eng. Chem. 40 (1948) 345–348.
[11] Y.-C. Tang, L. Pauling, Acta Cryst. 5 (1952) 39–44.
[12] F.E. Wittig, P. Scheidt, Z. Phys. Chem., NF 28 (1961) 120–142.
[13] E. Scheil, H.L. Lukas, Z. Metallkd. 52 (1961) 417–422.
[14] E. Kundys, J. Terpilowski, E. Zaleska, Archiwum Hutnictwa 7 (1962) 233–241.
[15] S.J. Stachura, T.G. Lenz, G. Burnet, Trans. Vacuum Metallur. Conf. (1964) 2–17.
[16] S. Nagasaki, A. Maesono, Private Communication, quoted by: M. Ide, K. Yonemitsu and T. Sato, Trans. Jpn. Inst. Metals 9 (1968) 363–366.
[17] B. Predel, R. Mohs, Z. Metallkd. 60 (1969) 606–609.
[18] B. Predel, W. Schürmann, Mater. Sci. Eng. 6 (1970) 303–312.
[19] L.Ya. Lyubman, S.Yu. Senyuta, V.S. Esyutin, L.Ya. Nurgaliev, Vak. Protsessy Tsvet. Met. (1971) 109–114.
[20] H.L. Lukas, unpublished measurements.
[21] S. Nakazawa, A. Yazawa, Nippon Kinzoku Gakkaishi 40 (1976) 715–722.
[22] R.M. Abbasov, A.O. Mekhrabov, R.A. Mustafaev, K.G. Binnatov, Azerb. Politekh. Inst. Im. Ildryma, Baku, USSR. Izvest. Vyssh. Ucheb. Zaved., Fiz. 119 (1976) 11–14.
[23] A.T. Dinsdale, Calphad 15 (1991) 317–425.
[24] W. Badawi, M. El-Talbi, A.M. Gun, Bull. Chem. Soc. Jpn. 63 (1990) 1795–1800.
[25] H.L. Lukas, S.G. Fries, J. Phase Equil. 13 (1992) 532–541.
[26] B. Jansson, M. Schalin, M. Selleby, B. Sundman, The thermo-calc database system, in: C.W. Bale, G.A. Irons (Eds.), Computer Software in Chemical and Extractive Metallurgy, The Met. Soc. of CIM, Quebec, 1993, pp. 57–71.
[27] Q. Li, H. Nguyen, H. Jamgotchian, B. Billia, Acta Metall. Mater. 43 (1995) 1271–1278.
[28] B. Sundman, I. Ansara, Calculation of solidification paths for multicomponent systems, in: K. Hack (Ed.), The SGTE Casebook, The Institute of Metals, UK, 1996, pp. 94–98.